Letters

A New Coupling Structure and Position Detection Method for Segmented Control Dynamic Wireless Power Transfer Systems

Xiaofei Li, Jiefeng Hu, *Senior Member, IEEE*, Heshou Wang, Xin Dai, *Member, IEEE*, and Yue Sun, *Member, IEEE*

***Abstract*—In this letter, a new coupling structure for dynamic wireless power transfer (DWPT) systems is proposed. Bipolar coils are symmetrically placed on the transmitter unipolar coils, resulting in natural decoupling between the bipolar coils and the unipolar coils. This special structure can mitigate the self-couplings between the adjacent unipolar transmitter coils and hence facilitate the design of the compensation circuit. Another remarkable advantage of this design is that it can lead to a stable mutual coupling between the transmitter array and the receiver when the receiver moves along the transmitter, making it a natural fit for DWPT applications. Furthermore, to reduce the electromagnetic interference and power loss, an automatic segmented control scheme is implemented, and a position detection method by monitoring the primary current is developed. The feasibility of the proposed coupling structure and the position detection method are verified on a laboratory prototype with 72-V output voltage. The experimental results show that the power fluctuation is within $\pm 2.5\%$, and system efficiency is around 90%. (This letter is accompanied by a video demonstrating the experimental test).**

***Index Terms*—Dynamic wireless power transfer (DWPT), mutual coupling, position detection, segmented control.**

I. Introduction

RECENTLY, more and more attention has been paid to electric vehicle (EV) charging using wireless power transfer (WPT) techniques because of their merits of convenience and safety [1]–[4]. The efficiency of a WPT system can reach up to 96%, which makes it comparable with traditional wire-based chargers [5]. Generally, EVs can be charged wirelessly not only when they are parked (i.e., stationary WPT), but also when they are moving [i.e., dynamic wireless power transfer (DWPT)] [6], [7]. As DWPT can contribute to extended driving range and reduced battery capacity, it has become a promising technology in EVs [8].

According to the sizes of the transmitter coils and receiver coils, DWPT systems can be divided into two types [6], [8]: first, long-track-transmitter type, where multiple receivers can be charged at the same time; and, second, short-multiple-transmitter type, where multiple transmitter coils are arranged in an array to charge the receiver. The advantage of the first type is the simple circuit structure. Nevertheless, its disadvantages are also obvious, such as high electromagnetic interference (EMI) and low coupling coefficient between transmitter and receiver coils. These lead to lower efficiency of the system. In contrast, for the second type, since the transmitters can be turned ON or OFF according to the position of the receiver, lower EMI and higher efficiency can be achieved [6]–[8].

Generally, to design a low EMI and high efficient DWPT system with the short-multiple-transmitter type, the following three aspects need to be considered.

1) The self-couplings between the transmitters should be small so that the compensation circuit design can be straightforward [8].
2) The mutual coupling between the transmitter array and the receiver should be relatively stable for stable the power output [6].
3) The position detection is needed so that the segmented control can be implemented to reduce EMI and power loss [6].

Self-coupling usually exists between adjacent transmitters. To reduce the self-coupling, one solution is to utilize the refined magnetic coupler. In [6], unipolar and bipolar structures are used as adjacent transmitters, which makes the self-couplings between the transmitters naturally small. In [4], the self-couplings between transmitters are mitigated by using refined inductor–capacitor–capacitor (*LCC*) compensators. Furthermore, self-coupling usually appears when the two transmitters are close to each other. Therefore, another way to reduce the self-coupling is to put the transmitters far away from each other. For

Manuscript received October 30, 2019; revised December 1, 2019 and December 23, 2019; accepted December 26, 2019. Date of publication December 30, 2019; date of current version March 13, 2020. This work was supported in part by The Hong Kong Polytechnic University under Grant G-YBZ4, in part by Hong Kong Innovation and Technology Commission under Grant ITS/281/17, in part by Hong Kong Research Grants Council under Grant PolyU252040/17E, in part by National Key R&D Program of China by MOST under Grant 2018YFB0106300, and in part by National Natural Science Foundation of China under Grant 51777022. *(Corresponding author: Jiefeng Hu.)*

X. Li, X. Dai, and Y. Sun are with the School of Automation, Chongqing University, Chongqing 400044, China (e-mail: 569411680@qq.com; toybear@vip.sina.com; syue06@cqu.edu.cn).

J. Hu is with the School of Science, Engineering and Information-Technology, Federation University, Ballarat, VIC 3350, Australia (e-mail: eejerryhu@gmail.com).

H. Wang is with the Department of Electrical Engineering, The Hong Kong Polytechnic University, Hong Kong (e-mail: 16104772g@connect.polyu.hk).

This letter has supplementary downloadable material available at http://ieeexplore.ieee.org, provided by the authors.

Color versions of one or more of the figures in this article are available online at http://ieeexplore.ieee.org.

Digital Object Identifier 10.1109/TPEL.2019.2963438

instance, self-couplings can be reduced effectively when the distance between the adjacent transmitters is about 30% of the transmitter length [9]. However, large distance between the adjacent transmitters raises another issue, i.e., the power pulsation phenomenon caused by the fluctuating mutual coupling between the transmitter array and the receiver [10].

For the second consideration in short-multiple-transmitter type DWPT systems, to keep the mutual coupling between the transmitter array and the receiver stable, Lu *et al*. [8] optimizes the size of the receiver coil. By ignoring the edge effects, during the movement, the variation of the coupling coefficient is only $\pm 2.1\%$, and the power pulsation can be maintained within $\pm 2.9\%$. Nevertheless, self-couplings between the transmitters still exist, which poses challenges in designing the compensation circuit. Li *et al*. [6] proposes a new magnetic coupler to reduce the mutual coupling variation. Unipolar and bipolar coils are placed alternately to form the transmitter array, whereas unipolar and bipolar coils are overlapped and connected in series on the receiver side. With this coupling structure, during the movement, the mutual inductance fluctuation is within $\pm 2\%$, and the power pulsation can also be achieved with only $\pm 2\%$ fluctuation. However, the position detection method, which is crucial to implement the automatic segmented control, is not illustrated in detail.

Regarding the position detection, conventionally optic or ultrasonic sensors can be employed to detect the position of the receiver. These sensors need to be installed in specific locations, and they may be affected by surrounding environment [11]. Recently, some research works have demonstrated that the position of the receiver can be estimated by the mutual inductance [11], [12], leading to effective position detection. However, these works mainly focus on stationary WPT systems without further considering DWPT applications.

To fill the technical gaps mentioned above, in this letter, a new coupling structure is proposed. Bipolar coils are used to mitigate the self-couplings between the adjacent unipolar transmitter coils. Since bipolar coils and unipolar coils are naturally decoupled, the stable mutual coupling between the transmitter array and the receiver, and hence stable power output, can be achieved. Furthermore, a position detection method by monitoring the primary current is developed to implement the automatic segmented control.

II. Proposed Coupling Structure With Stable Mutual Coupling

A. Proposed Coupling Structure to Cancel the Self-Coupling

Fig. 1(a) shows the proposed coupling structure with five unipolar transmitter coils, labeled L_{TQ1} to L_{TQ5}. L_{RQ} is the unipolar receiver coil. The transmitter coils and the receiver coil are with the same specifications. To make full use of the coil length, unipolar transmitter coils are placed closely next to each other. As a result, there are self-couplings between the adjacent unipolar coils, though those between the nonadjacent unipolar coils can be neglected [8], as indicated from the data at the upper-right corner in Table I. These coupling coefficients are measured in the experiment, and the coil specifications are shown in Fig. 1(b). Since that the polarity of the coupling

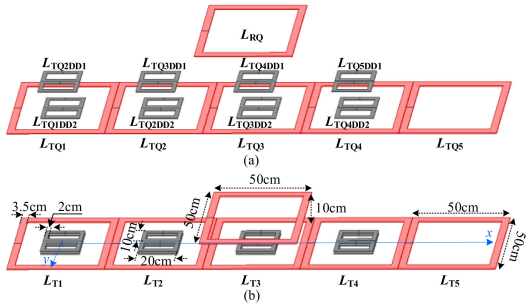

Fig. 1. (a) Proposed coupling structure. (b) Sizes of the coupling structure.

TABLE I
Measured Self-Coupling Coefficients

	$L_{\mathrm{T1}}(L_{\mathrm{TQ1}})$	$L_{\mathrm{T2}}(L_{\mathrm{TQ2}})$	$L_{\mathrm{T3}}(L_{\mathrm{TQ3}})$	$L_{\mathrm{T4}}(L_{\mathrm{TQ4}})$	$L_{\mathrm{T5}}(L_{\mathrm{TQ5}})$
$L_{\mathrm{T1}}(L_{\mathrm{TQ1}})$		-0.1188	-0.0086	-0.0017	-0.0004
$L_{\mathrm{T2}}(L_{\mathrm{TQ2}})$	0.0003		-0.1185	-0.0085	-0.0017
$L_{\mathrm{T3}}(L_{\mathrm{TQ3}})$	-0.0070	0.0006		-0.1185	-0.0086
$L_{\mathrm{T4}}(L_{\mathrm{TQ4}})$	-0.0014	-0.0065	0.0005		-0.1189
$L_{\mathrm{T5}}(L_{\mathrm{TQ5}})$	-0.0003	-0.0013	-0.0066	0.0002	

coefficient depends on the direction of the magnetic flux linkage coupled from one coil to the other, these self-coupling coefficients are negative [8], and they can be shown as

$$k_{\mathrm{LTQ}ij} = \frac{M_{\mathrm{LTQ}ij}}{L_{\mathrm{TQ}i}L_{\mathrm{TQ}j}} \tag{1}$$

where $M_{\mathrm{LTQ}ij}$ is the mutual inductance between $L_{\mathrm{TQ}i}$ and $L_{\mathrm{TQ}j}$, ($i = 1, 2, \ldots, 5$, $j = 1, 2, \ldots, 5$, $i \neq j$) and it equals to $M_{\mathrm{LTQ}ji}$.

To eliminate the self-couplings between the adjacent unipolar transmitter coils, bipolar coils are added. Specifically, (L_{TQ1DD2}, L_{TQ2DD1}), (L_{TQ2DD2}, L_{TQ3DD1}), (L_{TQ3DD2}, L_{TQ4DD1}), and (L_{TQ4DD2}, L_{TQ5DD1}) with positive self-couplings are used to cancel the mutual couplings between (L_{TQ1}, L_{TQ2}), (L_{TQ2}, L_{TQ3}), (L_{TQ3}, L_{TQ4}), and (L_{TQ4}, L_{TQ5}), respectively. The self-coupling coefficients between bipolar coils $L_{\mathrm{TQ}mDD2}$ and $L_{\mathrm{TQ}(m+1)DD1}$ ($m = 1, 2, \ldots, 4$) can be defined as

$$k_{\mathrm{LTQDD}m(m+1)} = \frac{M_{\mathrm{LTQDD}m(m+1)}}{L_{\mathrm{TQ}m\mathrm{DD2}}L_{\mathrm{TQ}(m+1)\mathrm{DD1}}} \tag{2}$$

where $M_{\mathrm{LTQDD}m(m+1)}$ is the mutual inductance between $L_{\mathrm{TQ}mDD2}$ and $L_{\mathrm{TQ}(m+1)DD1}$.

Such bipolar coils are placed in overlap at the central of the unipolar transmitter coils, as depicted in Fig. 1(b). As a result, the mutual-couplings between the unipolar coils and bipolar coils can be neglected [6]. (L_{TQ1DD2}, L_{TQ1}), (L_{TQ2DD1}, L_{TQ2DD2}, L_{TQ2}), (L_{TQ3DD1}, L_{TQ3DD2}, L_{TQ3}), (L_{TQ4DD1}, L_{TQ4DD2}, L_{TQ4}), and (L_{TQ5DD1}, L_{TQ5}) are connected in series to form L_{T1}, L_{T2}, L_{T3}, L_{T4}, and L_{T5}, respectively. The mathematical relations between the self-inductances can be derived as

$$L_{\mathrm{T}i} = L_{\mathrm{TQ}i} + \sum_{k=1}^{2} L_{\mathrm{TQ}i\mathrm{DD}k} \tag{3}$$

where $i = 1, 2, \ldots, 5$ and L_{TQ1DD1}, L_{TQ5DD2} do not exist, i.e., $L_{\mathrm{TQ1DD1}} = L_{\mathrm{TQ5DD2}} = 0\ \mu\mathrm{H}$.

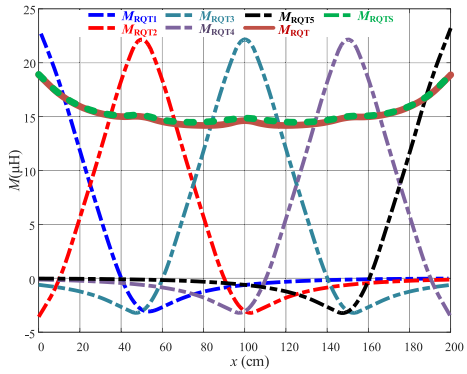

Fig. 2. Measured mutual inductances (x indicates the distance between the receiver and transmitter #1).

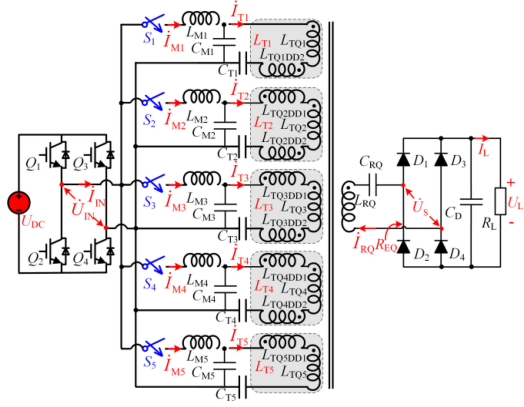

Fig. 3. Circuit diagram of the proposed WPT system.

Thus, according to (1)–(3), by optimizing coil specifications, the self-couplings between adjacent transmitters (i.e., L_{T1}, L_{T2}, L_{T3}, L_{T4}, and L_{T5}) can be eliminated. In this letter, the coils are made of 600-strand Litz wires with a diameter of 5 mm. The number of turns for unipolar transmitter and receiver coils is 7, whereas that for bipolar transmitter coils is 4. The measured self-couplings between L_{T1}, L_{T2}, L_{T3}, L_{T4}, L_{T5} are listed in the lower-left corner of Table I, showing that the self-couplings are neglectable. Consequently, the design of the compensation circuits is much more straightforward.

B. Stable Mutual Coupling and Segmented Control Logic

Fig. 2 shows the measured mutual inductances when the receiver moves along the x-axis. $M_{\mathrm{RQT}i}$ represents the mutual inductance between L_{RQ} and $L_{\mathrm{T}i}$ ($i = 1, 2, \ldots, 5$). The total mutual inductance between the transmitter array and the receiver is defined as M_{RQT}, which can be obtained as

$$M_{\mathrm{RQT}} = \sum_{i=1}^{5} M_{\mathrm{RQT}i}. \tag{4}$$

It is seen from Fig. 2 that M_{RQT} is relatively stable, especially in the middle section, i.e., 50 cm $\leq x \leq$ 150 cm, where the coupling fluctuation is within $\pm 1.7\%$.

When the receiver moves along the transmitter, specified transmitters will be turned ON/OFF accordingly, in order to reduce EMI and power loss [6]. According to Fig. 2, M_{RQT5} is almost zero when 0 cm $\leq x \leq$ 100 cm, whereas M_{RQT1} is almost zero when 100 cm $\leq x \leq$ 200 cm. Therefore, the segmented control logic is as follows. When x is smaller than 100 cm, transmitters #1–#4 are energized. When x is larger than 100 cm, transmitters #2–#5 are energized. In other words, transmitter #1 will be turned OFF and transmitter #5 will be turned ON once the receiver begins to move away from the transmitter #3. M_{RQTS} indicates the total mutual inductance when the segmented control is utilized

$$M_{\mathrm{RQTS}} = \begin{cases} \sum_{i=1}^{4} M_{\mathrm{RQT}i} & 0\ \mathrm{cm} \leq x \leq 100\ \mathrm{cm} \\ \sum_{i=2}^{5} M_{\mathrm{RQT}i} & 100\ \mathrm{cm} < x \leq 200\ \mathrm{cm}. \end{cases} \tag{5}$$

From Fig. 2, it is seen that M_{RQTS} is also relatively stable in the middle section, i.e., 50 cm $\leq x \leq$ 150 cm, where the coupling fluctuation is within $\pm 2.0\%$. In the following analysis, the middle section is therefore considered for segmented control.

III. Circuit Topology and System Control

A. Circuit Topology

The circuit diagram of the proposed DWPT system is shown in Fig. 3. Five *LCC* compensation topologies are used to compensate the transmitters, whereas series (S) compensation topology is used to compensate the receiver. S_i ($i = 1, 2, \ldots, 5$) is an ac switch that turns ON/OFF the ith transmitter.

To simplify the analysis, the parasitic resistances of the coils are ignored, and the power semiconductors are assumed to be ideal. The compensation variables for the five transmitters are assumed to be the same, i.e., $L_M = L_{\mathrm{M}i}$, ($i = 1, 2, \ldots, 5$). The compensation capacitors should satisfy the following equations:

$$\begin{aligned} C_{\mathrm{M}i} &= \left(\omega^2 L_{\mathrm{M}i}\right)^{-1} C_{\mathrm{T}i} = \left[\omega^2 \left(L_{\mathrm{T}i} - L_{\mathrm{M}i}\right)\right]^{-1} \\ C_{\mathrm{RQ}} &= \left(\omega^2 L_{\mathrm{RQ}}\right)^{-1} \end{aligned} \tag{6}$$

where ω is the operating angular frequency, $\omega = 2\pi f$, and f is the operating frequency of the system.

By utilizing the Kirchhoff's voltage law, according to the relationship between the input and output voltage of the inverter and rectifier [6], the following equations can be derived:

$$\begin{cases} \dot{U}_{\mathrm{IN}} = \frac{2\sqrt{2}}{\pi} U_{\mathrm{DC}} \angle 0^0 \\ \dot{U}_{\mathrm{IN}} = \left(jX_{\mathrm{LM}i} - jX_{\mathrm{CM}i}\right) \dot{I}_{\mathrm{M}i} + jX_{\mathrm{CM}i} \dot{I}_{\mathrm{T}i} \\ 0 = \left(jX_{\mathrm{LT}i} - jX_{\mathrm{CT}i} - jX_{\mathrm{CM}i}\right) \dot{I}_{\mathrm{T}i} + jX_{\mathrm{CM}i} \dot{I}_{\mathrm{M}i} \\ \qquad - jX_{\mathrm{MRQT}i} \dot{I}_{\mathrm{RQ}} + \delta \\ 0 = -jX_{\mathrm{MRQTS}} \dot{I}_{\mathrm{T}} + \left(jX_{\mathrm{LRQ}} - jX_{\mathrm{CRQ}} + R_{\mathrm{EQ}}\right) \dot{I}_{\mathrm{RQ}} \\ \dot{U}_S = R_{\mathrm{EQ}} \dot{I}_{\mathrm{RQ}} \\ U_L = \frac{\pi\sqrt{2}}{4} U_S \end{cases} \tag{7}$$

where U_S is the root mean square value of $\dot{U}_S$, $R_{\mathrm{EQ}} = 8R_L(\pi^2)^{-1}$, and symbol X represents the reactance. The detailed

definitions are as follows:

$$\begin{cases} X_{\mathrm{LM}i} = \omega L_{\mathrm{M}i} \quad X_{\mathrm{CM}i} = 1/\omega C_{\mathrm{M}i} \quad X_{\mathrm{LT}i} = \omega L_{\mathrm{T}i} \\ X_{\mathrm{CT}i} = 1/\omega C_{\mathrm{T}i} \quad X_{\mathrm{LRQ}} = \omega L_{\mathrm{RQ}} \quad X_{\mathrm{CRQ}} = 1/\omega C_{\mathrm{RQ}} \\ X_{\mathrm{MRQT}i} = \omega M_{\mathrm{RQT}i} \quad X_{\mathrm{MRQTS}} = \omega M_{\mathrm{RQTS}}. \end{cases} \tag{8}$$

As can be seen from (7), δ can be solved as

$$\delta = \begin{cases} j\left(X_{\mathrm{MLTQDD}i(i+1)} - X_{\mathrm{MLTQ}i(i+1)}\right)\dot{I}_{\mathrm{T}(i+1)} & i = 1 \\ j\left(X_{\mathrm{MLTQDD}(i-1)i} - X_{\mathrm{MLTQ}(i-1)i}\right)\dot{I}_{\mathrm{T}(i-1)} & \\ +j\left(X_{\mathrm{MLTQDD}i(i+1)} - X_{\mathrm{MLTQ}i(i+1)}\right)\dot{I}_{\mathrm{T}(i+1)} & i = 2,3,4 \\ j\left(X_{\mathrm{MLTQDD}(i-1)i} - X_{\mathrm{MLTQ}(i-1)i}\right)\dot{I}_{\mathrm{T}(i-1)} & i = 5 \end{cases} \tag{9}$$

where $X_{\mathrm{MLTQDD}i(i+1)}$, $X_{\mathrm{MLTQ}i(i+1)}$, $X_{\mathrm{MLTQDD}(i-1)i}$, and $X_{\mathrm{MLTQ}(i-1)i}$ are the corresponding reactance of $M_{\mathrm{LTQDD}i(i+1)}$, $M_{\mathrm{LTQ}i(i+1)}$, $M_{\mathrm{LTQDD}(i-1)i}$, and $M_{\mathrm{LTQ}(i-1)i}$, which can be solved as

$$\begin{cases} X_{\mathrm{MLTQDD}i(i+1)} = \omega M_{\mathrm{LTQDD}i(i+1)} \\ X_{\mathrm{MLTQ}i(i+1)} = \omega M_{\mathrm{LTQ}i(i+1)} \\ X_{\mathrm{MLTQDD}(i-1)i} = \omega M_{\mathrm{LTQDD}(i-1)i} \\ X_{\mathrm{MLTQ}(i-1)i} = \omega M_{\mathrm{LTQ}(i-1)i}. \end{cases} \tag{10}$$

By substituting (10) into (9), and considering that the self-couplings between adjacent unipolar coils are canceled by the added bipolar coils, as shown in Table I, it can be derived that the effects of self-couplings are eliminated and hence δ is negligible. Then, by substituting (6) and (8) into (7), one can obtain

$$\dot{I}_T = \dot{I}_{\mathrm{T}i} = \frac{\dot{U}_{\mathrm{IN}}}{j\omega L_{\mathrm{M}i}}, \quad U_L = \frac{M_{\mathrm{RQTS}} U_{\mathrm{DC}}}{L_{\mathrm{M}}}$$

$$\dot{I}_{\mathrm{M}i} = \frac{M_{\mathrm{RQT}i} M_{\mathrm{RQTS}} \dot{U}_{\mathrm{IN}}}{{L_{\mathrm{M}i}}^2 R_{\mathrm{EQ}}} \quad (i = 1, 2, \ldots, 5). \tag{11}$$

It is obvious from (11) that $\dot{I}_{\mathrm{T}i}$and U_L are irrelevant to the load. For U_L, once U_{DC} and L_M are determined, when the receiver moves along the transmitter, the dynamic U_L is only related to the segmented total mutual inductance M_{RQTS}. Consequently, U_L can remain stable as long as M_{RQTS} is kept stable.

B. System Control With Position Detection

As mentioned in Section II-C, the segmented control position is $x = 100$ cm, i.e., the receiver is fully aligned with the third transmitter, at which M_{RQT3} reaches its maximum value as can be seen from Fig. 2. Equation (11) implies that, since M_{RQTS} is relatively stable, once U_{DC}, L_M is determined, with constant R_L during the movement, $\dot{I}_{\mathrm{M}i}$only relates to $M_{\mathrm{RQT}i}$ (i = 1, 2, …, 5). Therefore, by finding the maximum value of$|\dot{I}_{M3}|$, the segmented control point can be identified. The relationship between $|\dot{I}_{M3}|$and x with different R_L is illustrated in Fig. 4. When the receiver moves along the transmitter array, the controller records $|\dot{I}_{M3}|$in every sampling step k. For every consecutive three sampling values, if the middle sampling point is the largest, the segmented control position is found. This means that transmitter #1 should be turned OFF and transmitter #5 should be turned ON at that corresponding position. For better illustration, a flowchart is presented in Fig. 5 to explain the segmented control point determination.

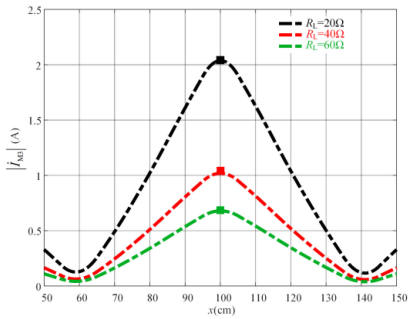

Fig. 4. Relationship between $|\dot{I}_{M3}|$and x with different R_L.

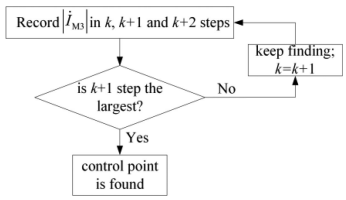

Fig. 5. Flowchart to find the segmented control point.

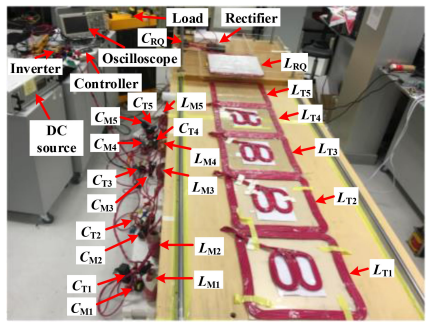

Fig. 6. Experimental setup.

TABLE II
SYSTEM PARAMETERS

U_{DC}	$L_{\mathrm{T1}}, L_{\mathrm{T5}}$	$L_{\mathrm{T2}}, L_{\mathrm{T3}}, L_{\mathrm{T4}}$	L_{RQ}	C_{RQ}
140V	64.33μH	73.00μH	58.04μH	60.41nF
f	$C_{\mathrm{T1}}, C_{\mathrm{T5}}$	$C_{\mathrm{T2}}, C_{\mathrm{T3}}, C_{\mathrm{T4}}$	L_{M}	C_{M}
85kHz	97.39nF	78.48nF	28.33μH	123. 75μH

IV. EXPERIMENTAL VERIFICATIONS

Fig. 6 shows the laboratory prototype built. The parameters of the system are listed in Table II. Bidirectional switches ($S_1 \sim S_5$) are constructed by low-cost ac relays HF161F-W from Hongfa Technology [13].

First, the load-independent output voltage is tested. Fig. 7 shows the dynamic response of the system when R_L changes from 20 to 40 Ω and back to 20 Ω. It can be seen that U_L can

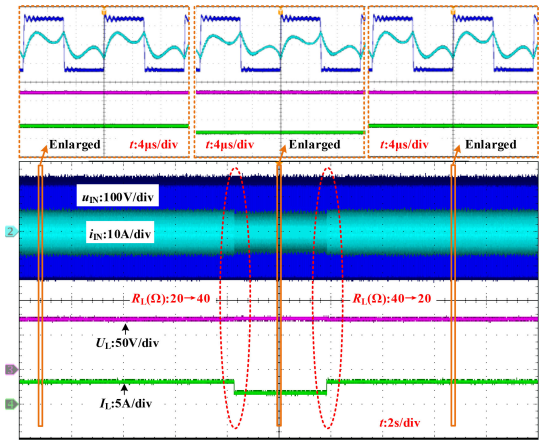

Fig. 7. Dynamic response when R_L change.

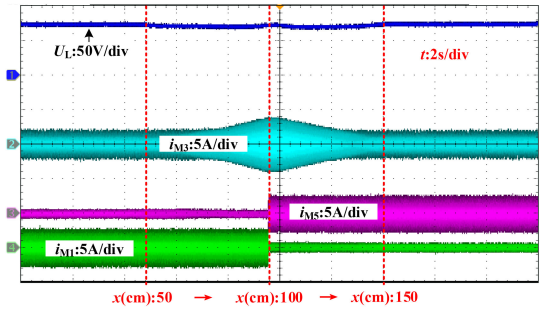

Fig. 8. Dynamic response when receiver moves along the transmitter array.

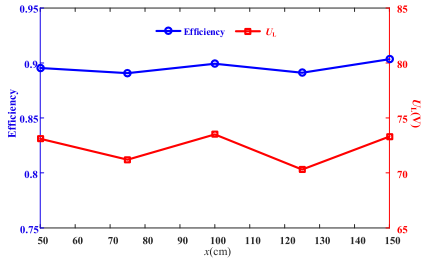

Fig. 9. Output voltage and system efficiency results during the movement.

remain constant at 72 V, which proves the load-independent constant voltage output of the system. From the enlarged view, it is observed that $u_{\rm IN}$ and $i_{\rm IN}$ are nearly in phase, which indicates that most of the reactive power can be eliminated. In addition, $i_{\rm IN}$ lags slightly behind $u_{\rm IN}$, which is conductive for the system to achieve zero-voltage switching [14].

Fig. 8 shows the dynamic response of the system when the receiver moves along the transmitter array. There is no closed-loop control for the output voltage. The position of the receiver is changed from $x = 50$ cm to $x = 150$ cm. Load R_L is fixed at 20 Ω. The system starts at $x = 50$ cm with transmitter #1 ON and transmitter #5 OFF (i.e., i_{M5} is zero). At $x = 100$ cm, once the maximum point of $|\dot{I}_{M3}|$is identified, the controller conducts the segmented control, i.e., transmitter #1 OFF (i_{M1} is zero) and transmitter #5 ON. The output voltage and system efficiency during the movement are replotted in Fig. 9. It is seen that the output voltage is relatively stable during the movement, and the fluctuation is within ±2.5%. The efficiency of the system is around 90% in the tests. Refer to a video recording of the experimental test attached in this submission to better observe the system performance including segmented control.

V. Conclusion

In this letter, a coupling structure for DWPT systems with stable output power is proposed. Bipolar coils are used to mitigate the self-couplings between the adjacent unipolar transmitter coils. Bipolar coils are symmetrically placed on the unipolar coils, resulting in the fact that bipolar coils and unipolar coils are naturally decoupled. Thus, the stable mutual coupling between the transmitter array and the receiver, and hence stable output power, can be achieved. The automatic segmented control is utilized to reduce the extra EMI and power loss, based on the proposed primary current monitoring position detection method. An experimental prototype is built to verify the feasibility of the proposed coupling structure and the position detection method. The experimental results show that with the segmented control, the power fluctuation is within ±2.5%, and system efficiency is around 90%.

References

[1] C. C. Mi, G. Buja, S. Y. Choi, and C. T. Rim, "Modern advances in wireless power transfer systems for roadway powered electric vehicles," *IEEE Trans. Ind. Electron.*, vol. 63, no. 10, pp. 6533–6545, Oct. 2016.

[2] S. Y. Choi, B. W. Gu, S. Y. Jeong, and C. T. Rim, "Advances in wireless power transfer systems for roadway-powered electric vehicles," *IEEE J. Emerg. Sel. Topics Power Electron.*, vol. 3, no. 1, pp. 18–36, Mar. 2015.

[3] G. A. Covic and J. T. Boys, "Modern trends in inductive power transfer for transportation applications," *IEEE J. Emerg. Sel. Topics Power Electron.*, vol. 1, no. 1, pp. 28–41, Mar. 2013.

[4] F. Farajizadeh, M. Vilathgamuwa, D. Jovanovic, P. Jayathurathnage, G. Ledwich, and U. Madawala, "Expandable N-legged converter to drive closely spaced multi transmitter wireless power transfer systems for dynamic charging," *IEEE Trans. Power Electron.*, vol. 35, no. 4, pp. 3794–3806, Apr. 2020.

[5] J. Deng, F. Lu, S. Li, T. Nguyen, and C. Mi, "Development of a high efficiency primary side controlled 7 kW wireless power charger," in *Proc. IEEE Int. Elect. Veh. Conf.*, 2014, pp. 1–6.

[6] Y. Li *et al.*, "A new coil structure and its optimization design with constant output voltage and constant output current for electric vehicle dynamic wireless charging," *IEEE Trans. Ind. Informat.*, vol. 15, no. 9, pp. 5244–5256, Sep. 2019.

[7] S. Zhou and C. C. Mi, "Multi-paralleled LCC reactive power compensation networks and their tuning method for electric vehicle dynamic wireless charging," *IEEE Trans. Ind. Electron.*, vol. 63, no. 10, pp. 6546–6556, Oct. 2016.

[8] F. Lu, H. Zhang, H. Hofmann, and C. C. Mi, "A dynamic charging system with reduced output power pulsation for electric vehicles," *IEEE Trans. Ind. Electron.*, vol. 63, no. 10, pp. 6580–6590, Oct. 2016.

[9] J. M. Miller, P. T. Jones, J. Li, and O. C. Onar, "ORNL experience and challenges facing dynamic wireless power charging of EV's," *IEEE Circuits Syst. Mag.*, vol. 15, no. 2, pp. 40–53, May 2015.

[10] K. Lee, Z. Pantic, and S. M. Lukic, "Reflexive field containment in dynamic inductive power transfer systems," *IEEE Trans. Power Electron.*, vol. 29, no. 9, pp. 4592–4602, Sep. 2014.

[11] X. Dai, J. C. Jiang, and J. Q. Wu, "Charging area determining and power enhancement method for multiexcitation unit configuration of wirelessly dynamic charging EV system," *IEEE Trans. Ind. Electron.*, vol. 66, no. 5, pp. 4086–4096, Oct. 2016.

[12] Z. You and S. O'Driscoll, "Implant positioning system using mutual inductance," in *Proc. Annu. Int. Conf. IEEE Eng. Med. Biol. Soc.*, 2012, pp. 751–754.

[13] Hongfa Technology, "HF161F-W," [Online]. Available: http://www.hong-fa.com/pro/html/HF161F-W_en.html

[14] X. Qu, H. Han, S. C. Wong, C. K. Tse, and W. Chen, "Hybrid IPT topologies with constant current or constant voltage output for battery charging applications," *IEEE Trans. Power Electron.*, vol. 30, no. 11, pp. 6329–6337, Nov. 2015.